44th AIAA/ASME/SAE/ASEE Joint Propulsion Conference & Exhibit
21 - 23 July 2008, Hartford, CT

AIAA 2008-4832

Energy Based Solutions of the Bidirectional Vortex

Tony Saad* and Joseph Majdalani†
University of Tennessee Space Institute, Tullahoma, TN 37388

In this study, two families of solutions are developed for the bidirectional vortex in a cylindrical chamber using Lagrangian optimization. Our optimization procedure is applied to the kinetic energy of the system and is prompted by the idea that a fluid will follow the path of least kinetic energy in the absence of forcing. Once the solution with least kinetic energy is obtained, other more energetic profiles that satisfy the problem's boundary conditions are exposed. At the outset, two types of solutions, I and II, are established. These expansions either lag or exceed in system energy the exact Vyas-Majdalani solution (Vyas, A. B. and Majdalani, J., "Exact Solution of the Bidirectional Vortex," *AIAA Journal*, Vol. 44, No. 10, 2006, pp. 2208-2216). Furthermore, the two types of solutions exhibit quantum-like energy states that depend on an energy power index, *q*. When *q* is increased, the two classes of solutions asymptotically approach the Vyas-Majdalani model while maintaining either lower or higher kinetic energies. From this perspective, the fundamental solution can be viewed as a stable saddle function to which all other solutions converge. Parametrically, the energy-based solutions are found to be dependent on the chamber aspect ratio, injection flowrate, and energy power index. The present analysis expands our understanding of the bidirectional vortex and paves the way for a stability framework that incorporates unsteady wave coupling with the mean flow.

Nomenclature

a	= chamber radius
E_V	= total volumetric kinetic energy
$\mathscr{E}$	= kinetic energy density, $E_V/(\kappa^2 L^3)$
L	= normalized chamber length, L_0 / a
$\bar{Q}_i$	= total inlet volumetric flowrate
Q_i	= normalized inlet volumetric flowrate, $\bar{Q}_i/(Ua^2)$
r , z	= normalized radial and axial coordinate, $\bar{r} / a$, $\bar{z} / a$
$\boldsymbol{u}$	= normalized velocity $(\bar{u}, \bar{v}, \bar{w})/U$
U	= mean inflow velocity $\bar{v}(a, L_0)$
η	= action variable, $(2n+1)\pi r^2$
κ	= inflow parameter, $Q_i/2\pi L$
ρ	= density

Indices

$\bar{}$	= overbars denote dimensional variables
$^-$	= denotes Type I solutions
$^+$	= denotes Type II solutions

I. Introduction

HIGHLY rotating flows are among the most feature-rich motions that are encountered in the analysis of swirling fluid formations. From the devastating power of tornadoes and hurricanes that occur in nature[1] to the vortex-

*Doctoral Research Assistant, Department of Mechanical, Aerospace and Biomedical Engineering. Member AIAA.

†H. H. Arnold Chair of Excellence in Advanced Propulsion, Department of Mechanical, Aerospace and Biomedical Engineering. Member AIAA. Fellow ASME.

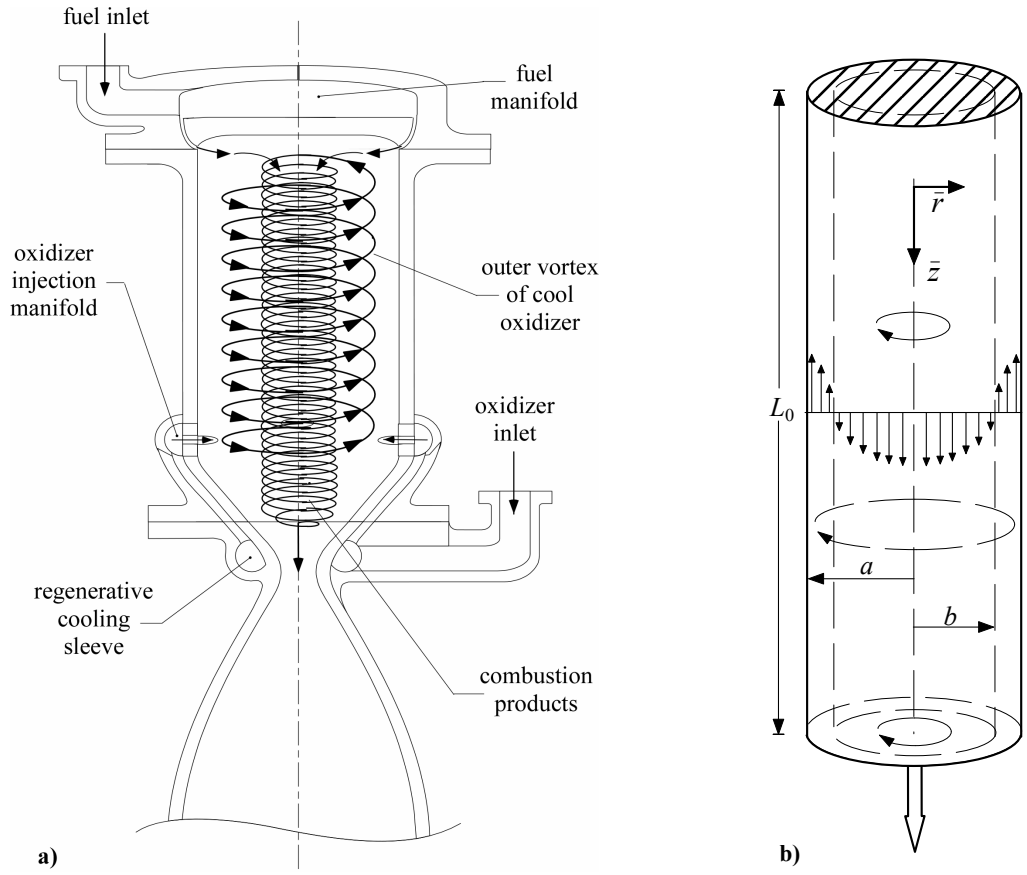

Figure 1. Side-by-side comparison between the Vortex Combustion Cold-Wall Chamber (VCCWC) by Chiaverini *et al.*[3,4] and the simulated vortex chamber used in conjunction with the present mathematical model.

fired thrust chambers[2-4] that are developed for space exploration, highly swirling flows exhibit some of the most intriguing and predictively daunting characteristics. In this vein, a substantial amount of research has been invested in studying both confined[5-12] and unconfined swirling configurations.[13-21] Among them is our particular interest in the confined bidirectional vortex, a bipolar fluid structure that emerges in the Vortex Combustion Cold-Wall Chamber (VCCWC) developed by Chiaverini *et al.*[3,4] (see Fig. 1a).

One of the earliest models to describe this problem may be attributed to Vyas and Majdalani;[5] Majdalani and Rienstra[6] have also focused on spherical geometry and the extraction of new classes of nonlinear solutions not exposed previously. Other relevant solutions include those describing the presence of multiple mantles,[12] viscous core corrections,[11] tangential boundary layers,[22] and both radial and axial sidewall boundary layers.[8] Numerical and experimental investigations of the vortex chamber have also been performed by Anderson *et al.*,[2] Rom, Anderson and Chiaverini,[23] Murray *et al.*,[24] Sauer *et al.*[25] (using LOX/RP-1), Chiaverini *et al.*[4] (using O2/H2), Fang, Majdalani and Chiaverini,[26,27] (using both cold and reactive flow conditions), and others. Due to the striking similarity between a bidirectional vortex and a cyclonic flowfield, other pertinent models include those by Fontein and Dijksman,[28] Smith,[29,30] Bloor and Ingham,[31,32] and Kelsall.[33] Elegant simulations of cyclonic flows have also been performed by Boysan, Ayers and Swithenbank,[34] Hsieh and Rajamani,[35] Hoekstra, Derksen and Van den Akker,[36] Derksen and Van den Akker,[37] and Hu *et al.*[38]

The present article applies the concept of Lagrangian optimization to the set of profiles describing cyclonic motion, often referred to as bidirectional vortex motion in the propulsion community. Such a framework has been shown to be valuable in deriving new families of solutions for a variety of physical problems in which a basic mean flowfield is established. In this context, Majdalani and Saad[39,40] have derived approximate analytical solutions for flows mimicking the internal gaseous motion in solid and hybrid rocket motors. They have also provided accurate representations for slab-rocket chambers simulating both solid and hybrid rockets[41,42] with arbitrary headwall

injection. In these studies, the Lagrangian optimization technique led to additional families of solutions with discrete energy signatures.[40,42] The energy-based profiles displayed either smoother or steeper profiles that could be associated with turbulent or compressible flow motions.[43] In this article, we extend our analysis to the more complex bidirectional vortex chamber in which the streamlines experience both flow reversal near the head-end and rotation about the centerline. This extension enables us to better understand the intricate similarities that affect both injection and swirl driven thrust chambers.

II. Mathematical Model

Following Vyas and Majdalani,[5] the inviscid bidirectional vortex can be modeled as a cylindrical chamber of length L_0 and radius a with uniform tangential injection along its sidewall (Fig. 1b). The flow is assumed to be steady, inviscid, inert and rotational. The solution domain extends from the headwall to the virtual nozzle attachment at the exit where $\bar{z} = L_0$. At the injection port, the flow enters the chamber at a given flowrate $\bar{Q}_i$. This stream then undergoes a double helical motion prompted by the rotation of fluid layers with the lowest pressure occurring along the centerline. In what follows, we seek to approximate solutions that may exist besides the basic bidirectional vortex model. In particular, we hope to identify those particular solutions that require lower or higher energies to excite.

A. Equations

We start with the inviscid Euler flow equations,

$$\frac{1}{\bar{r}}\frac{\partial(\bar{r}\bar{u})}{\partial\bar{r}} + \frac{1}{\bar{r}}\frac{\partial\bar{v}}{\partial\theta} + \frac{\partial\bar{w}}{\partial\bar{z}} = 0 \tag{1}$$

$$\bar{u}\frac{\partial\bar{u}}{\partial\bar{r}} + \frac{\bar{v}}{\bar{r}}\frac{\partial\bar{u}}{\partial\theta} + \bar{w}\frac{\partial\bar{u}}{\partial\bar{z}} - \frac{\bar{v}^2}{\bar{r}} = -\frac{1}{\rho}\frac{\partial\bar{p}}{\partial\bar{r}} \tag{2}$$

$$\bar{u}\frac{\partial\bar{v}}{\partial\bar{r}} + \frac{\bar{v}}{\bar{r}}\frac{\partial\bar{v}}{\partial\theta} + \bar{w}\frac{\partial\bar{v}}{\partial\bar{z}} + \frac{\bar{u}\,\bar{v}}{\bar{r}} = -\frac{1}{\rho\bar{r}}\frac{\partial\bar{p}}{\partial\theta} \tag{3}$$

$$\bar{u}\frac{\partial\bar{w}}{\partial\bar{r}} + \frac{\bar{v}}{\bar{r}}\frac{\partial\bar{w}}{\partial\theta} + \bar{w}\frac{\partial\bar{w}}{\partial\bar{z}} = -\frac{1}{\rho}\frac{\partial\bar{p}}{\partial\bar{z}} \tag{4}$$

where u, v, and w stand for the radial, azimuthal, and axial velocities, respectively. Axisymmetry about the centerline is useful in eliminating tangential derivatives. Furthermore, the absence of friction between fluid layers enables us to assume a tangential velocity that is independent of the axial direction.[5,44] This typical set of assumptions helps to transform the governing equations into

$$\frac{1}{\bar{r}}\frac{\partial(\bar{r}\bar{u})}{\partial\bar{r}} + \frac{\partial\bar{w}}{\partial\bar{z}} = 0 \tag{5}$$

$$\bar{u}\frac{\partial\bar{u}}{\partial\bar{r}} + \bar{w}\frac{\partial\bar{u}}{\partial\bar{z}} - \frac{\bar{v}^2}{\bar{r}} = -\frac{1}{\rho}\frac{\partial\bar{p}}{\partial\bar{r}} \tag{6}$$

$$\bar{u}\frac{\partial\bar{v}}{\partial\bar{r}} + \frac{\bar{u}\,\bar{v}}{\bar{r}} = 0 \tag{7}$$

$$\bar{u}\frac{\partial\bar{w}}{\partial\bar{r}} + \bar{w}\frac{\partial\bar{w}}{\partial\bar{z}} = -\frac{1}{\rho}\frac{\partial\bar{p}}{\partial\bar{z}} \tag{8}$$

B. Boundary Conditions

These are physically connected to

(a) tangential inflow at the sidewall;
(b) vanishing axial flow at the headend;
(c) no radial flow at the centerline;
(d) no radial inflow at the sidewall; and
(d) an axial source that matches the tangential stream entering at the base.

These conditions can be expressed as

$$\begin{cases} \overline{v}(a,L)=U & \text{(average circumferential velocity)} \\ \overline{w}(\overline{r},0)=0 & \text{(vanishing axial flow at the headend)} \\ \overline{u}(0,\overline{z})=0 & \text{(no radial flow at the centerline)} \\ \overline{u}(a,\overline{z})=0 & \text{(no radial inflow at the sidewall)} \\ \int_b^a \overline{w}(\overline{r},L_0)\overline{r}\,\mathrm{d}\overline{r}=\overline{Q}_i=UA_i & \text{(axial inflow matching tangential source)} \end{cases} \tag{9}$$

C. Normalization

For simplicity, we normalize all variables according to

$$z=\frac{\overline{z}}{a};\ r=\frac{\overline{r}}{a};\ \boldsymbol{u}=\frac{\overline{\boldsymbol{u}}}{U};\ p=\frac{\overline{p}}{\rho U^2};\ \psi=\frac{\overline{\psi}}{a^2U_w} \tag{10}$$

$$Q_i=\frac{\overline{Q}_i}{Ua^2}=\frac{A_i}{a^2};\ Q_o=\frac{\overline{Q}_o}{Ua^2};\ \nabla=a\overline{\nabla};\ \beta=\frac{b}{a} \tag{11}$$

Here $U=\overline{v}(a,L_0)=\overline{Q}_i/A_i$ is the average injection velocity and b stands for the nozzle radius and mantle location. For steady inviscid motion, the vorticity transport equation reduces to

$$\nabla\times(\boldsymbol{u}\times\boldsymbol{\Omega})=0;\quad \boldsymbol{\Omega}=\nabla\times\boldsymbol{u} \tag{12}$$

Similarly, the dimensionless boundary conditions take the form

$$\begin{cases} v(1,L)=1 & \text{(tangential inflow)} \\ w(r,0)=0 & \text{(vanishing axial flow at the headend)} \\ u(0,z)=0 & \text{(no radial flow at the centerline)} \\ u(1,z)=0 & \text{(no radial inflow at the sidewall)} \\ \int_0^{2\pi}\int_0^{\beta} w(r,L)\,r\,\mathrm{d}r\,\mathrm{d}\theta=Q_i & \text{(axial inflow matching tangential source)} \end{cases} \tag{13}$$

D. Decoupling of Euler's Equations

The governing equations can be decoupled from the tangential velocity component via Eq. (7), namely,

$$u\left(\frac{\partial v}{\partial r}+\frac{v}{r}\right)=0 \quad \text{or} \quad v=\frac{1}{r} \tag{14}$$

This relation represents a free vortex. The singularity at the centerline is due to the absence of friction, a necessary ingredient to attenuate the tangential velocity at the centerline.[5] This undesirable deficiency may be circumvented by adding viscous core corrections, as shown by Vyas and Majdalani.[22] Their result may be expressed as function of a vortex Reynolds number V, where

$$v=\begin{cases} \dfrac{1}{r}\left[1-e^{-\frac{1}{4}Vr^2}-e^{-\frac{1}{4}\left(\frac{1}{6}\pi^2-1\right)V\left(1-r^2\right)}\right]; & 0<z<L;\quad V\equiv\dfrac{\rho UA_i}{L_0\mu} \\ \dfrac{1}{r}\left(1-e^{-\frac{1}{4}Vr^2}\right); & z=L \quad \text{(tangential injection at entry)} \end{cases} \tag{15}$$

With the tangential velocity decoupled from the axial and radial equations, we are left with a reduced axisymmteric problem that can be further simplified by making use of the stream function.

E. Vorticity-Stream Function Approach

The Stokes stream function may be introduced through

$$u=-\frac{1}{r}\frac{\partial\psi}{\partial z} \qquad \text{and} \qquad w=\frac{1}{r}\frac{\partial\psi}{\partial r} \tag{16}$$

As usual, substitution into Eq. (12) requires that

$$\Omega=rF(\psi)=C^2r\psi \tag{17}$$

Despite the non-uniqueness of this expression, it satisfies Eq. (12). Then by inserting Eq. (17) into the vorticity equation, one obtains the characteristic equation for this problem, specifically

$$\frac{\partial^2\psi}{\partial z^2}+\frac{\partial^2\psi}{\partial r^2}-\frac{1}{r}\frac{\partial\psi}{\partial r}+C^2r^2\psi=0 \tag{18}$$

with

$$\begin{cases}\text{(a)} & z=0: \quad w=0; \quad \partial\psi/\partial r=0;\\ \text{(b)} & r=0: \quad u=0; \quad \partial\psi/\partial z=0;\\ \text{(d)} & r=1: \quad u=0; \quad \partial\psi/\partial z=0;\\ \text{(d)} & \int_0^{2\pi}\int_0^{\beta}\left(\partial\psi/\partial r\right)\mathrm{d}r\,\mathrm{d}\theta=Q_i.\end{cases} \tag{19}$$

When Eq. (18) is solved by separation of variables, one finds

$$\psi(r,z)=(\alpha z+\varphi)[A\cos(Cr^2)+B\sin(Cr^2)] \tag{20}$$

III. Energy Triggered Solutions

A. Solution by Eigenfunction Expansions

The boundary conditions may be applied sequentially. Starting with Eq. (19)a

$$\frac{\partial\psi(r,0)}{\partial r}=\varphi[\tfrac{1}{2}C\,rA\cos(Cr^2)+\tfrac{1}{2}C\,rB\sin(Cr^2)]=0 \tag{21}$$

we get $\varphi=0$. Next, application of Eq. (19)b yields

$$\frac{\partial\psi(0,z)}{\partial z}=\alpha A=0 \tag{22}$$

Since $\alpha\neq 0,$ we take $A=0$. Without loss in generality, we set $B=1$ and rewrite the remaining solution as

$$\psi(r,z)=\alpha z\sin(Cr^2) \tag{23}$$

At this point, application of Eq. (19)c returns

$$\frac{\partial\psi(1,z)}{\partial z}=\alpha\sin(C)=0 \tag{24}$$

and so $\sin(C)=0$. In order to derive energy-based profiles, we introduce eigensolutions that observe this constraint. Therefore, instead of limiting our attention to the fundamental solution given by $C=\pi,$ [5] we consider the general form of *C* as

$$C=C_k=(k+1)\pi;\; k=\{0,1,2,...,\infty\}\in\mathbb{N} \tag{25}$$

Using $C_k=(k+1)\pi$ enables us to sum over infinite eigenfunctions, thus setting the stage for the energy optimization technique to be implemented. We proceed by disregarding negative integers that lead to self-cancellation, and sum over all possible eigensolutions

$$\psi(r,z)=\sum_{k=0}^{\infty}\alpha_k z\sin\left[(k+1)\pi r^2\right];\qquad \text{where}\qquad \psi_k(r,z)=\alpha_k z\sin\left[(k+1)\pi r^2\right] \tag{26}$$

The last boundary condition provides the constraint for $\{\alpha_k\}$. From Eq. (19)d we obtain

$$\int_0^{2\pi}\int_0^{\beta}L\sum_{k=0}^{\infty}2(k+1)\pi\alpha_k\cos\left[(k+1)\pi r^2\right]r\,\mathrm{d}r\,\mathrm{d}\theta=Q_i \tag{27}$$

or

$$\sum_{k=0}^{\infty}\alpha_k\sin\left[(k+1)\pi\beta^2\right]=\frac{Q_i}{2\pi L}\equiv\kappa \tag{28}$$

B. Mantle Location

To make headway, we must first determine the value of β that sets the theoretical location of the mantle. The mantle is defined as that rotating layer where the axial velocity vanishes.[5] Its locus is the root of $w(\beta,z)=0.$ For our solution, we have

$$\sum_{k=0}^{\infty}(k+1)\alpha_k\cos\left[(k+1)\pi\beta^2\right]=\alpha_0\cos\left(\pi\beta^2\right)+2\alpha_1\cos\left(2\pi\beta^2\right)+...+(k+1)\alpha_k\cos\left[(k+1)\pi\beta^2\right]=0 \tag{29}$$

Each term in the series has to vanish identically if Eq. (29) is to be satisfied. However, since $\{\alpha_k\}$ is nonzero then the cosine terms in Eq. (29) should be null for the same value of β. This can be extracted from the first term as

$$\cos(\pi\beta^2) = 0 \quad \text{or} \quad \beta = 1/\sqrt{2} \tag{30}$$

This value coincides, as it should, with the single mantle location derived by Vyas and Majdalani.[5] Interestingly, when $\beta = 1/\sqrt{2}$ is substituted back into Eq. (29), only terms with even indices vanish. This guides us to ignore odd indices in the Fourier-type summation and write $k = 2n$, $n = \{0,1,2,...,\infty\} \in \mathbb{N}$. The corresponding constants take the form

$$C_k = (k+1)\pi \rightarrow C_n = (2n+1)\pi;\ n = \{0,1,2,...,\infty\} \in \mathbb{N} \tag{31}$$

Note that the refinement in the choice of $\{C_n\}$ does not alter the character of the solution, but only remaps the interval of $\{C_n\}$ to odd multiples of π. The ensuing series expansion becomes

$$\psi(r,z) = \sum_{n=0}^{\infty} \alpha_n z \sin\left[(2n+1)\pi r^2\right] \tag{32}$$

With the mantle location determined, Eq. (28) becomes

$$\sum_{n=0}^{\infty} (-1)^n \alpha_n = \kappa \tag{33}$$

We now proceed to determine an auxiliary equation that can be imposed on $\{\alpha_n\}$.

C. Energy Optimization

Clearly, an infinite number of possibilities exist that may, in principle, satisfy Eq. (33), depending on the behavior of $\{\alpha_n\}$. One of these choices may be arrived at by optimizing the total kinetic energy in the chamber. The underlying principle projects that a flow may choose the path of least or most energy requirement. To test this behavior, we evaluate the local kinetic energy at (r,z) for each eigensolution using

$$E_n(r,z) = \tfrac{1}{2}\boldsymbol{u}_n^2 = \tfrac{1}{2}(u_n^2 + w_n^2) \tag{34}$$

where each mode is an exact solution bearing the form

$$u_n = -\frac{\alpha_n}{r}\sin\eta; \quad w_n = 2(2n+1)\pi\,\alpha_n z\cos\eta\,; \quad \eta \equiv (2n+1)\pi r^2 \tag{35}$$

Note that the tangential velocity is not included in the evaluation of E_n because it is decoupled from the remaining velocity components and hence independent of n. Stated differently, the contribution of the tangential velocity to the kinetic energy remains fixed irrespective of the energy level being considered. By assuming a system of eigensolutions with individual kinetic energies, their cumulative energy can be written locally as

$$E_L = \sum_{n=0}^{\infty} E_n(r,z) = \tfrac{1}{2}\sum_{n=0}^{\infty}\left[\alpha_n^2 r^{-2}\sin^2\eta + 4\pi^2(2n+1)^2\alpha_n^2 z^2\cos^2\eta\right] \tag{36}$$

The total kinetic energy in the chamber volume V may be calculated by integrating the local kinetic energy over the length and chamber cross-section. One puts

$$E_V = \int_0^{2\pi}\int_0^L\int_0^1 E_L\, r\,\mathrm{d}r\,\mathrm{d}z\,d\theta = \pi\sum_{n=0}^{\infty}\int_0^L\int_0^1\left[\alpha_n^2 r^{-2}\sin^2\eta + 4\pi^2(2n+1)^2\alpha_n^2 z^2\cos^2\eta\right] r\,\mathrm{d}r\,\mathrm{d}z \tag{37}$$

Straightforward evaluation and simplification over the chamber volume yields

$$E_V = \tfrac{1}{12}L^3\pi^3\sum_{n=0}^{\infty}\alpha_n^2 a_n + L^{-2}\pi^{-2}\alpha_n^2 b_n \tag{38}$$

where

$$a_n = 4(2n+1)^2; \quad b_n = 3\,\mathrm{Cin}\left[2(2n+1)\pi\right] \tag{39}$$

Here $\mathrm{Cin}(x) = \int_0^x (1-\cos t)\,t^{-1}\,\mathrm{d}t$ is the entire cosine integral. At this point, one may seek the extremum of the total kinetic energy subject to the fundamental constraint

$$\sum_{n=0}^{\infty}(-1)^n\alpha_n = \kappa \tag{40}$$

The method of Lagrangian multipliers may be employed by introducing the constrained energy function

$$g = E_V + \lambda\left[\sum_{n=0}^{\infty}(-1)^n\alpha_n - \kappa\right] \tag{41}$$

Equation (41) can then be maximized or minimized by imposing $\nabla g(\alpha_0, \alpha_1, \alpha_2, ..., \lambda) = 0$. In shorthand notation, one sets

$$\nabla g(\alpha_n, \lambda) = 0 \quad n = \{0, 1, 2..., \infty\} \tag{42}$$

Subsequently, the constrained energy function may be differentiated with respect to each of its variables to obtain

$$\frac{\partial g}{\partial \alpha_n} = \frac{\pi^3 L^3}{12}\left(2\alpha_n a_n + 2\pi^{-2}L^{-2}\alpha_n b_n\right) + (-1)^n\lambda = 0; \quad n = \{0, 1, 2..., \infty\} \tag{43}$$

$$\frac{\partial g}{\partial \lambda} = \sum_{n=0}^{\infty}(-1)^n\alpha_n - \kappa = 0 \tag{44}$$

Equation (43) can be solved for $\{\alpha_n\}$ in terms of λ such that

$$\alpha_n = -\frac{6\pi^{-3}L^{-3}(-1)^n\lambda}{a_n + \pi^{-2}L^{-2}b_n} \tag{45}$$

The outcome can be suitably substituted into Eq. (44) to procure

$$\lambda = -\frac{\pi^3 L^3\kappa}{6\sum_{n=0}^{\infty}(a_n + \pi^{-2}L^{-2}b_n)^{-1}} \tag{46}$$

When λ is inserted into Eq. (45), an expression for $\{\alpha_n\}$ is obtained, specifically,

$$\alpha_n = \frac{(-1)^n\kappa}{(a_n + \pi^{-2}L^{-2}b_n)\sum_{i=0}^{\infty}(a_i + \pi^{-2}L^{-2}b_i)^{-1}} \tag{47}$$

With this relation at hand, the total energy given by Eq. (38) is fully determined. Then from Eqs. (47) and (38) one can segregate κ. It is then useful to introduce a compact form of the energy density such as $\mathscr{E} = E_V/(\kappa^2 L^3)$. The long expression resulting for $\mathscr{E}$ is omitted here for the sake of brevity. Its asymptotic approximation will be presented instead.

By plotting $\mathscr{E}$ versus L in Fig. 2, one is able to estimate the energy requirements associated with the bidirectional vortex depending on the chamber length. One also finds that as the length of the chamber is increased at fixed radius, $\mathscr{E}$ approaches a constant asymptotic value of $\mathscr{E}_\infty^- = 8\pi/3 \simeq 8.3776$. A critical aspect ratio L_{cr} can be proposed beyond which the kinetic energy will vary by less than 1% from its final asymptotic value $\mathscr{E}_\infty^-$. Technically, we would have $\mathscr{E} - \mathscr{E}_\infty^- \le 0.01\,\mathscr{E}_\infty^-$. Thus, for a chamber with $L \ge L_{cr}$, one may safely assume that $L \to \infty$ in evaluating Eq. (47), as a less than 1% error will be entailed. The outcome of this approximation translates into a substantial reduction in complexity. The critical length can be calculated to be 3.95125 for the bidirectional vortex. This relatively small value for the critical length is fortuitous as existing vortex engines have comparable aspect ratios and, therefore, the simplification obtained by letting $L \to \infty$ can be implemented with a reasonable degree of approximation.

A simple case may be illustrated for a vortex chamber with an aspect ratio that exceeds L_{cr}. Letting $L \to \infty$, Eq. (47) reduces to

$$\alpha_n = (-1)^n\kappa\left(a_n\sum_{i=0}^{\infty}a_i^{-1}\right)^{-1} = \frac{8(-1)^n\kappa}{\pi^2(2n+1)^2} \tag{48}$$

This simple relation fully satisfies the fundamental constraint expressed through Eq. (40).

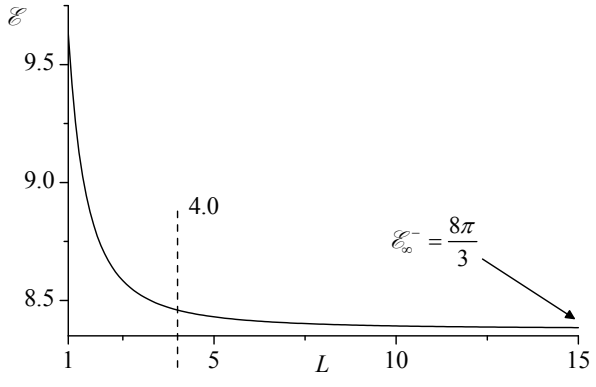

Figure 2. Kinetic energy variation vs. chamber length *L*.

D. Least Kinetic Energy Solution

It should be noted that the optimization technique based on Lagrangian multipliers enables us to identify the problem's extremum with no indication of whether the outcome corresponds to a minimum or a maximum. A substitution of Eq. (48) into Eq. (38) is resorted to for

comparing the energy content of the present approximation to that of the Euler formulation given by Vyas and Majdalani.[5] We find that the strategy just pursued exposes the solution with least kinetic energy. When $L \to \infty$ the energy-minimized formulation that emerges from Eq. (26) reduces to

$$\psi(r,z) = \frac{8}{\pi^2}\kappa z \sum_{n=0}^{\infty} \frac{(-1)^n}{(2n+1)^2} \sin\left[(2n+1)\pi r^2\right] \tag{49}$$

Corresponding streamlines are illustrated in Fig. 3a. Using solid lines to denote the fundamental solution, the steepened curves are shown using broken lines. The energy-minimized solution exhibits steep curvatures that are reminiscent of those associated with turbulent or compressible flow motions.[43] The radial and axial velocities with least kinetic energy are obtained from Eq. (49) and posted in Table 1.

IV. Generalization

The solution that we have obtained reflects the least kinetic energy that the flow may be able to sustain. If a family of solutions could be envisioned with other energy states, then the particular solution that we have identified could be viewed as the datum for all possible permutations. Evidently, it would be valuable to identify other mean flow solutions that exhibit increasing levels of kinetic energy, specifically those leading to the flowfield with maximum energy. It would also be informative to rank the solution given by Vyas and Majdalani[5] according to its energy content. Being explicitly closed, the Vyas-Majdalani profile will be referred to as the Type 0 or baseline solution. In our quest for a generalization, we consider $L \geq 4$ and make use of Eq. (48) as a guide. We also recognize that the source of steepening stems from the main injection sequence, and thus $\{\alpha_n\}$ contains the key parameters that control the energy level for a given flowfield.

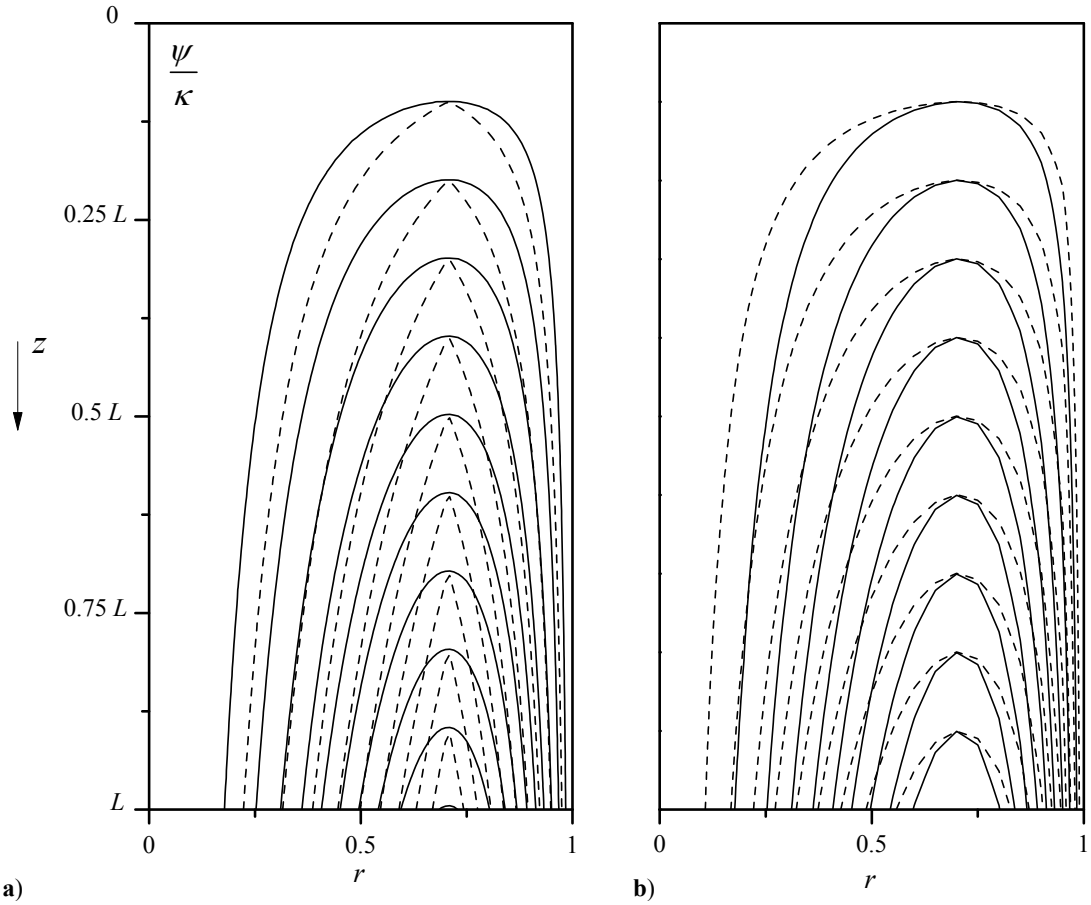

Figure 3. Flow streamlines for either (a) Type I solutions (left) with increasing energy levels or (b) Type II solutions (right) with decreasing energy levels.

Table 1. Solutions with least or most kinetic energies compared to the Vyas-Majdalani profile

Quantity	Type I (least KE)	Vyas-Majdalani[5]	Type II (most KE)
ψ	$\frac{8\kappa}{\pi^2} z \sum_{n=0}^{\infty} \frac{(-1)^n}{(2n+1)^2} \sin\eta$	$\kappa z \sin(\pi r^2)$	$\frac{\kappa}{\mathscr{C}} z \sum_{n=0}^{\infty} \frac{1}{(2n+1)^2} \sin\eta$
u	$-\frac{8\kappa}{\pi^2 r} \sum_{n=0}^{\infty} \frac{(-1)^n}{(2n+1)^2} \sin\eta$	$-\frac{\kappa}{r} \sin(\pi r^2)$	$-\frac{\kappa}{\mathscr{C} r} \sum_{n=0}^{\infty} \frac{1}{(2n+1)^2} \sin\eta$
w	$\frac{16\kappa}{\pi} z \sum_{n=0}^{\infty} \frac{(-1)^n}{(2n+1)} \cos\eta$	$2\pi\kappa z \cos(\pi r^2)$	$\frac{2\pi\kappa}{\mathscr{C}} z \sum_{n=0}^{\infty} \frac{1}{(2n+1)} \cos\eta$
ω_θ	0	$4\pi^2 \kappa r z \sin(\pi r^2)$	$\frac{2\pi^2 \kappa}{\mathscr{C}} rz \csc(\pi r^2)$

A. Type I Solutions with Increasing Energy Levels

Our objective here is to produce a family of solutions with valid sets of $\{\alpha_n\}$ that conform to the solution obtained through Lagrangian optimization. We begin by remarking that

$$\alpha_n = \frac{8(-1)^n \kappa}{\pi^2 (2n+1)^2} = \frac{(-1)^n \kappa A_2}{(2n+1)^2} \tag{50}$$

where $A_2 = 8/\pi^2$ is connected with the constraint given by Eq. (40). Similarly, the subscript may be linked to the power of $(2n+1)$ in the denominator. To generalize, we introduce the Type I family of solutions with

$$\alpha_n^-(q) = \frac{(-1)^n \kappa A_q}{(2n+1)^q}; \quad q \geq 2 \tag{51}$$

where $q = 2$ reproduces the state of least energy disbursement. This relation can be made to satisfy Eq. (40) when

$$\sum_{n=0}^{\infty} (-1)^n \frac{(-1)^n A_q}{(2n+1)^q} = 1 \quad \text{or} \quad A_q = \frac{1}{\sum_{n=0}^{\infty} (2n+1)^{-q}} = \frac{1}{\zeta(q)(1-2^{-q})}; \quad \zeta(q) = \textstyle\sum_{k=1}^{\infty} k^{-q} \tag{52}$$

Interestingly, Riemann's zeta function surfaces. Note that the $q \geq 2$ condition is needed to ensure series convergence down to the vorticity. Backward substitution enables us to collect the proper form of $\{\alpha_n\}$, namely,

$$\alpha_n^-(q) = \frac{(-1)^n (2n+1)^{-q} \kappa}{\sum_{k=0}^{\infty} (2k+1)^{-q}} = \frac{(-1)^n (2n+1)^{-q} \kappa}{\zeta(q)(1-2^{-q})}; \quad q \geq 2 \quad \text{(Type I)} \tag{53}$$

Here the exponent q represents the kinetic energy power index. The 'minus' sign in the superscript implies an energy state that is lower than the baseline case. With the form given by Eq. (53), one can plot the variation of the total kinetic energy versus the kinetic energy power index q. This plot is shown in Fig. 4a for several aspect ratios. Interestingly, as $q \to \infty$, the baseline solution is recovered. In fact, the analytical limit of Eq. (53) can be shown to be

$$\lim_{q\to\infty} \alpha_n^-(q) = \begin{cases} 1; & n = 0 \\ 0; & n = \{1, 2, ..., \infty\} \end{cases} \tag{54}$$

The elimination of all constants except for the first identically reproduces the baseline solution. The family of Type I expansions that are unraveled from Eq. (53) possess kinetic energies that are lower than the baseline. They can be bracketed between Eq. (49) and $\psi(r,z) = \kappa z \sin(\pi r^2)$.

B. Type II Solutions with Decreasing Energy Levels

To capture solutions with energies that exceed the baseline case, a modified formulation for $\{\alpha_n\}$ is in order. One may set

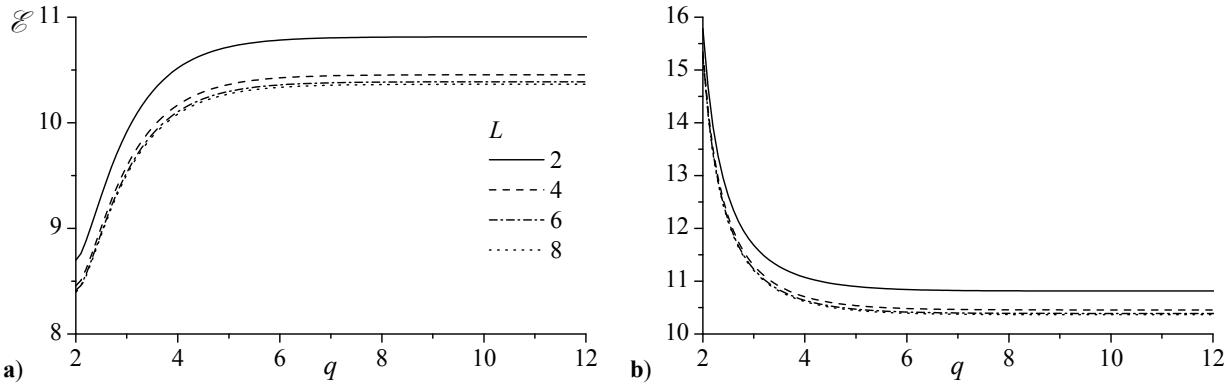

Figure 4. Total kinetic energy density in a vortex chamber for either (a) Type I solutions (left) with increasing energy levels or (b) Type II solutions (right) with decreasing energy levels. Results are for *L* = 2, 4, 6, and 8.

$$\alpha_n^+(q) = \frac{B_q \kappa}{(2n+1)^q}; \quad q \geq 2 \tag{55}$$

The key difference here stands in the exclusion of the $(-1)^n$ multiplier, a term that was previously retained in Eq. (50). Unless this term is lumped into B_q, no expansions can be constructed with energies that are higher than the baseline. In denoting Type II behavior, the 'plus' sign tagged in the superscript alludes to higher energies. Our remaining steps are similar to those used before. Substitution into Eq. (40) yields

$$\sum_{n=0}^{\infty} (-1)^n \frac{B_q}{(2n+1)^q} = 1 \quad \text{or} \quad B_q = \frac{1}{\sum_{n=0}^{\infty} (-1)^n (2n+1)^{-q}} = \frac{4^q}{\zeta(q, \frac{1}{4}) - \zeta(q, \frac{3}{4})} \tag{56}$$

where $\zeta(q,a) = \sum_{k=0}^{\infty} (k+a)^{-q}$ is Riemann's generalized zeta function. Equation (56) produces

$$\alpha_n^+(q) = \frac{(2n+1)^{-q} \kappa}{\sum_{k=0}^{\infty} (-1)^k (2k+1)^{-q}} = \frac{4^q (2n+1)^{-q} \kappa}{\zeta(q, \frac{1}{4}) - \zeta(q, \frac{3}{4})} \quad \text{(Type II)} \tag{57}$$

It can be shown that the Type II expansions issuing from Eq. (57) exhibit higher kinetic energies than the Type 0 solution. The variation of their kinetic energy with respect to q is illustrated in Fig. 4b for several aspect ratios. According to this form of $\{\alpha_n^+\}$, the model proposed by Vyas and Majdalani[5] is recoverable asymptotically by taking the limit as $q \to \infty$. So common to the two types of expansions obtained heretofore, the Vyas-Majdalani profile[5] seems to constitute a stable saddle function to which all series solutions quickly converge when their energies are either increased or decreased.

For the Type II expansions, when the energy level is fixed at $q = 2$, a simplification follows. Catalan's constant emerges in Eq. (57), namely, in the form

$$\mathscr{C} = \sum_{k=0}^{\infty} (-1)^k (2n+1)^{-2} \simeq 0.915966 \tag{58}$$

The streamlines corresponding to the solution with the most kinetic energy are plotted in Fig. 3b. The Type II approximation is seen to overshoot the baseline streamline curvature. We also note that in computing the kinetic energy density shown in Fig. 4, the large L approximation is only used in evaluating $\{\alpha_n\}$.

C. Velocity and Vorticity

The radial and axial velocities may be determined from

$$u = -\frac{\kappa}{r} \sum_{n=0}^{\infty} \alpha_n \sin \eta; \quad w = 2\kappa\pi \sum_{n=0}^{\infty} (2n+1) \alpha_n \cos \eta \tag{59}$$

These expressions are evaluated for the Type 0, I, and II cases ($q = 2$) and catalogued in Table 1. The effect of varying the energy power index on the velocity field is shown in Fig. 5 for the streamline turn angle as well as the radial and axial velocities. The turn angle is defined as

$$\theta(r) = \frac{180}{\pi} \tan^{-1}\left(-\frac{1}{z} \frac{u_z}{u_r} \right) \tag{60}$$

Finally, the vorticity may be determined from

$$\omega_\theta = \frac{\partial u}{\partial z} - \frac{\partial w}{\partial r} = 4\pi^2 rz \sum_{n=0}^{\infty} (2n+1)^2 \, \alpha_n \sin\eta \tag{61}$$

This is evaluated for the least and most kinetic energy formulations $(q = 2)$ as well as the reference case. These are also found in Table 1.

D. Asymptotic Behavior of the Kinetic Energy Density

The limit of the kinetic energy density as $L \to \infty$ can be written as

$$\mathscr{E}_\infty = \tfrac{1}{3}\pi^3 \sum_{n=0}^{\infty} (2n+1)^2 \, \alpha_n^2 = \mathscr{E}_\infty^\infty \sum_{n=0}^{\infty} (2n+1)^2 \, \alpha_n^2 \tag{62}$$

where $\mathscr{E}_\infty^\infty \equiv \pi^3 / 3 \simeq 10.335$ is the asymptotic limit of the kinetic energy of the Type 0 ($L \to \infty$ and $q \to \infty$). For the Type I solutions, substitution of Eq. (53) yields a closed-form expression, namely,

$$\mathscr{E}_\infty^- (q) = \mathscr{E}_\infty^\infty \left[\sum_{k=0}^{\infty} (2k+1)^{-q} \right]^{-2} \sum_{n=0}^{\infty} (2n+1)^{2-2q} = \mathscr{E}_\infty^\infty \frac{4^q - 4}{(2^q - 1)^2} \frac{\zeta(2q-2)}{[\zeta(q)]^2} \tag{63}$$

In like manner, for the Type II solutions, Eq. (57) leads to

$$\mathscr{E}_\infty^+ (q) = \mathscr{E}_\infty^\infty \left[\sum_{k=0}^{\infty} (-1)^k (2k+1)^{-q} \right]^{-2} \sum_{n=0}^{\infty} (2n+1)^{2-2q} = \mathscr{E}_\infty^\infty \frac{4^q (4^q - 4)\zeta(2q-2)}{[\zeta(q, \frac{1}{4}) - \zeta(q, \frac{3}{4})]^2} \tag{64}$$

Specific values of these limits are $\mathscr{E}_\infty^- (2) \simeq 8.377$, $\mathscr{E}_\infty^- (4) \simeq 10.053$, and $\mathscr{E}_\infty^- (6) \simeq 10.305$ for the Type I, and $\mathscr{E}_\infty^+ (2) \simeq 15.197$, $\mathscr{E}_\infty^+ (4) \simeq 10.583$, and $\mathscr{E}_\infty^+ (6) \simeq 10.362$ for the Type II. Both types approach $\mathscr{E}_\infty^\infty$ either from below or above. The energy level entertained with each power index may be extracted from Fig. 6. Evidently, all solutions with $q \geq 5$ are indiscernible from the fundamental Type 0 solution with an energy difference of less than

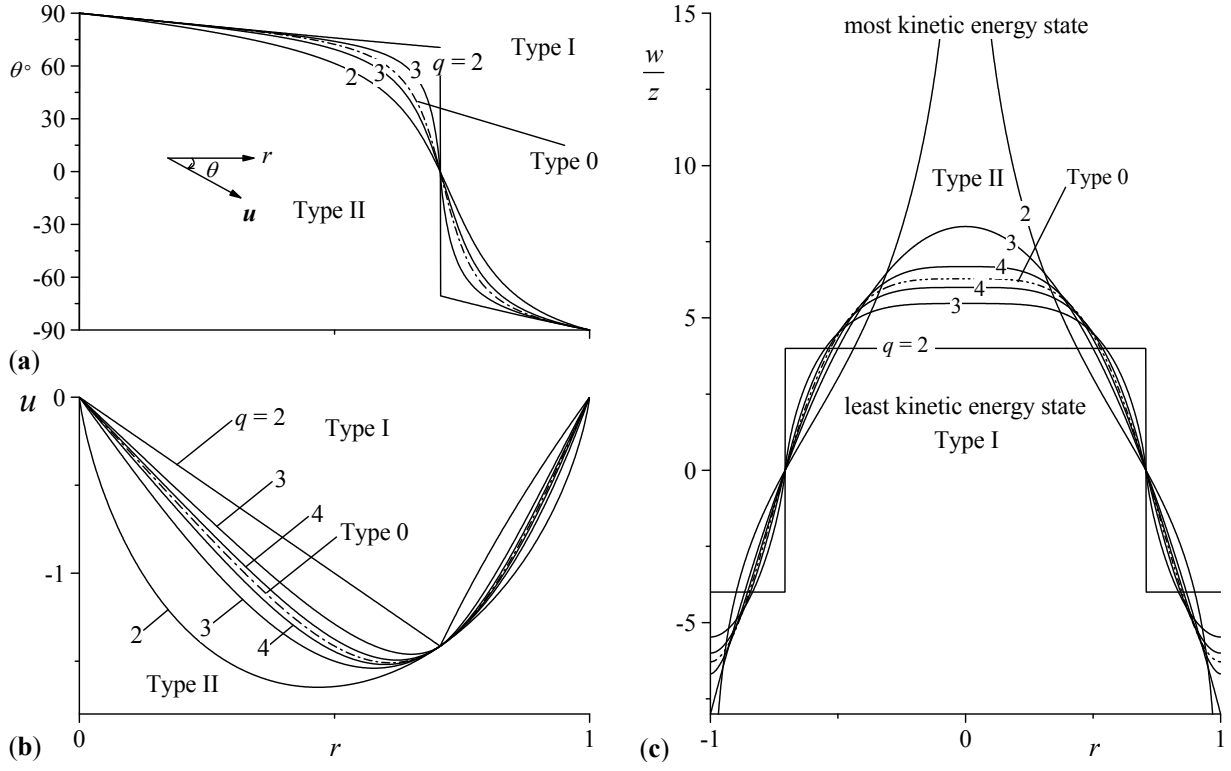

Figure 5. Effect of the energy power index on the velocity field for the flow with an inert headwall; (a) turn angle, (b) normal velocity, and (c) axial velocity.

1%. Each family of solutions exhibits a different range of higher or lower energies than the Type 0 solution. For example, the most noticeable Type I solutions are associated with $q = 2,\ 3$, and 4 with energies that are 81.1, 91.7, and 97.3% of the baseline solution. In a similar fashion, the Type II solutions exhibit energies that are 47.0, 8.08, and 2.40% higher. All other solutions are indiscernible from the Vyas-Majdalani profile.[5] The asymptotic limit of 10.335 is quickly recovered by both Type I and Type II solutions with differences of less than 0.287 and 0.265% at $q = 6$. Finally, the maximum energy range occurs at $q = 2$. This is the total allowable excursion in energy that the mean flow can undergo and may be estimated at $\left[\mathscr{E}_\infty^+(2) - \mathscr{E}_\infty^-(2)\right] / \mathscr{E}_\infty^\infty = 66.0\%$, an appreciable portion of the available energy.

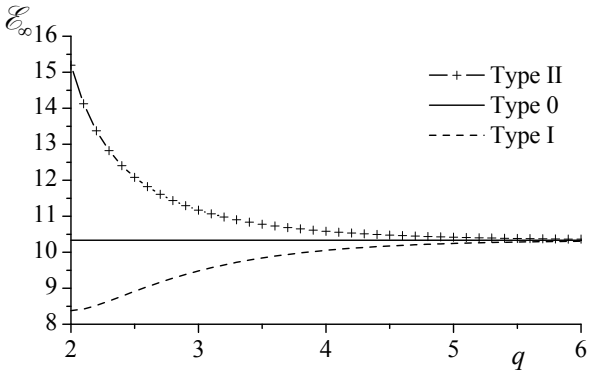

Figure 6. Asymptotic limits of the kinetic energy density showing rapid convergence of both Type I and Type II solutions to the Type 0 value of 10.335.

V. Conclusions

In the past four decades, vortex technology has been gaining interest almost evenly in the military and commercial sectors. Recently, an extension to a similar family of solutions has been carried out to improve the models for solid rocket motors and hybrids by incorporating arbitrary headwall injection and multiple energy-based solutions. In this article, we have applied the energy optimization technique to the bidirectional vortex chamber. We have shown that other solutions may be obtained, and these are accompanied by lower or higher kinetic energies that vary by up to 66% of their mean value. After identifying that $\alpha_n^- \sim (-1)^n (2n+1)^{-2}$ yields the profile with least kinetic energy, similar Type I solutions are unraveled in ascending order, $\alpha_n^- \sim (-1)^n (2n+1)^{-q};\ q > 2$, up to the reference model proposed by Vyas and Majdalani.[5] In all cases, the Vyas-Majdalani profile is asymptotically recovered in the limit as $q \to \infty$. In practice, most solutions become indiscernible from the reference case for $q \geq 5$. Interestingly, those obtained with $q = 2,\ 3$, and 4 exhibit energies that are 18.9, 8.28 and 2.73% lower than their remaining counterparts. When the same analysis is repeated using $\alpha_n^+ \sim (2n+1)^{-q};\ q \geq 2$, a complementary family of Type II solutions is identified with descending energy levels. Their most notable expansions correspond to $q = 2,\ 3$, and 4, with energies that are 47.0, 8.08, and 2.40% higher than the reference profile. Effectively, the Type I and II families converge to the Vyas-Majdalani[5] representation when their energies are augmented or reduced, respectively. In future work, experimental validation of the energy-based solutions will be invaluable as will be the use of the energy-based models to represent physically realistic flows.

Acknowledgments

This work was sponsored by the National Science Foundation through Grant No. CMMI-0353518. The senior author acknowledges valuable discussions with Dr. Grégoire Casalis, Professor and Director of the Doctoral School of Aeronautics and Astronautics, SUPAERO, and Research Director, Department of Aerodynamics and Energetics, ONERA, Toulouse, France. We also thank Dr. Martin J. Chiaverini, Lead Propulsion Engineer at Orbital Technologies Corporation, for his encouragement, suggestions, and technical support whenever needed.

References

[1]Penner, S. S., "Elementary Considerations of the Fluid Mechanics of Tornadoes and Hurricanes," *Acta Astronautica,* Vol. 17, 1972, pp. 351-362.

[2]Anderson, M. H., Valenzuela, R., Rom, C. J., Bonazza, R., and Chiaverini, M. J., "Vortex Chamber Flow Field Characterization for Gelled Propellant Combustor Applications," AIAA Paper 2003-4474, July 2003.

[3]Chiaverini, M. J., Malecki, M. J., Sauer, J. A., and Knuth, W. H., "Vortex Combustion Chamber Development for Future Liquid Rocket Engine Applications," AIAA Paper 2002-2149, July 2002.

[4]Chiaverini, M. J., Malecki, M. J., Sauer, J. A., Knuth, W. H., and Majdalani, J., "Vortex Thrust Chamber Testing and Analysis for O2-H2 Propulsion Applications," AIAA Paper 2003-4473, July 2003.

[5]Vyas, A. B., and Majdalani, J., "Exact Solution of the Bidirectional Vortex," *AIAA Journal,* Vol. 44, No. 10, 2006, pp. 2208-2216.

[6]Majdalani, J., and Rienstra, S. W., "On the Bidirectional Vortex and Other Similarity Solutions in Spherical Coordinates," *Journal of Applied Mathematics and Physics (ZAMP),* Vol. 58, No. 2, 2007, pp. 289-308.

[7]Reydon, R. F., and Gauvin, W. H., "Theoretical and Experimental Studies of Confined Vortex Flow," *The Canadian Journal of Chemical Engineering,* Vol. 59, 1981, pp. 14-23.

[8]Batterson, J. W., and Majdalani, J., "On the Boundary Layers of the Bidirectional Vortex," AIAA Paper 2007-4123 June 2007.

[9]Vatistas, G. H., Jawarneh, A. M., and Hong, H., "Flow Characteristics in a Vortex Chamber," *The Canadian Journal of Chemical Engineering,* Vol. 83, No. 6, 2005, pp. 425-436.

[10]Vatistas, G. H., Lin, S., and Kwok, C. K., "Theoretical and Experimental Studies on Vortex Chamber Flows," *AIAA Journal,* Vol. 24, No. 4, 1986, pp. 635-642.

[11]Vyas, A. B., Majdalani, J., and Chiaverini, M. J., "The Bidirectional Vortex. Part 2: Viscous Core Corrections," AIAA Paper 2003-5053, July 2003.

[12]Vyas, A. B., Majdalani, J., and Chiaverini, M. J., "The Bidirectional Vortex. Part 3: Multiple Solutions," AIAA Paper 2003-5054, July 2003.

[13]Eloy, C., and Le Dizès, S., "Three-Dimensional Instability of Burgers and Lamb-Oseen Vortices in a Strain Field," *Journal of Fluid Mechanics,* Vol. 378, No. 1, 1999, pp. 145-166.

[14]Escudier, M. P., "Vortex Breakdown - Observations and Explanations," *Progress in Aerospace Sciences,* Vol. 25, No. 2, 1988, pp. 189-229.

[15]Escudier, M. P., and Zehnder, N., "Vortex-Flow Regimes," *Journal of Fluid Mechanics,* Vol. 115, No. 1, 1982, pp. 105-121.

[16]Faler, J. H., and Leibovich, S., "Disrupted States of Vortex Flow and Vortex Breakdown," *Physics of Fluids,* Vol. 20, No. 9, 1977, pp. 1385-1400.

[17]Hall, M. G., "Vortex Breakdown," *Annual Review of Fluid Mechanics*, Vol. 41972, pp. 195-218.

[18]Long, R. R., "A Vortex in an Infinite Viscous Fluid," *Journal of Fluid Mechanics,* Vol. 11, No. 4, 1961, pp. 611-624.

[19]Sarpkaya, T., "New Model for Vortex Decay in the Atmosphere," *Journal of Aircraft,* Vol. 37, No. 1, 2000, pp. 53-61.

[20]Schmid, P. J., and Rossi, M., "Three-Dimensional Stability of a Burgers Vortex," *Journal of Fluid Mechanics,* Vol. 500, No. 1, 2004, pp. 103-112.

[21]Trapp, R. J., "A Clarification of Vortex Breakdown and Tornadogenesis," *Monthly Weather Review,* Vol. 128, No. 3, 2000, pp. 888-895.

[22]Vyas, A. B., and Majdalani, J., "Characterization of the Tangential Boundary Layers in the Bidirectional Vortex Thrust Chamber," AIAA Paper 2006-4888, July 2006.

[23]Rom, C. J., Anderson, M. H., and Chiaverini, M. J., "Cold Flow Analysis of a Vortex Chamber Engine for Gelled Propellant Combustor Applications," AIAA Paper 2004-3359, July 2004.

[24]Murray, A. L., Gudgen, A. J., Chiaverini, M. J., Sauer, J. A., and Knuth, W. H., "Numerical Code Development for Simulating Gel Propellant Combustion Processes," JANNAF May 2004.

[25]Sauer, J. A., Malecki, M. M., Knuth, W. H., Chiaverini, M. J., and Hall, C. D., "Development of a LOX/RP-1 Vortex Combustion Cold-Wall Thrust Chamber Assembly," AAIA Paper 2002-4144, July 2002.

[26]Fang, D., Majdalani, J., and Chiaverini, M. J., "Simulation of the Cold-Wall Swirl Driven Combustion Chamber," AIAA Paper 2003-5055, July 2003.

[27]Fang, D., Majdalani, J., and Chiaverini, M. J., "Hot Flow Model of the Vortex Cold Wall Liquid Rocket," AIAA Paper 2004-3676, July 2004.

[28]Fontein, F. J., and Dijksman, C., *Recent Developments in Mineral Dressing*, Institution of Mining and Metallurgy, London, 1953, p. 229.

[29]Smith, J. L., "An Experimental Study of the Vortex in the Cyclone Separator," *Journal of Basic Engineering-Transactions of the ASME*, 1962, pp. 602-608.

[30]Smith, J. L., "An Analysis of the Vortex Flow in the Cyclone Separator," *Journal of Basic Engineering-Transactions of the ASME*, 1962, pp. 609-618.

[31]Bloor, M. I. G., and Ingham, D. B., "Theoretical Investigation of the Flow in a Conical Hydrocyclone," *Transactions of the Institution of Chemical Engineers,* Vol. 51, No. 1, 1973, pp. 36-41.

[32]Bloor, M. I. G., and Ingham, D. B., "The Flow in Industrial Cyclones," *Journal of Fluid Mechanics,* Vol. 178, No. 1, 1987, pp. 507-519.

[33]Kelsall, D. F., "A Study of Motion of Solid Particles in a Hydraulic Cyclone," *Transactions of the Institution of Chemical Engineers,* Vol. 30, 1952, pp. 87-103.

[34]Boysan, F., Ayers, W. H., and Swithenbank, J., "A Fundamental Mathematical Modelling Approach to Cyclone Design," *Institute of Chemical Engineers,* Vol. 60, 1982, pp. 222-230.

[35]Hsieh, K. T., and Rajamani, R. K., "Mathematical Model of the Hydrocyclone Based on Physics of Fluid Flow," *AIChE Journal,* Vol. 37, No. 5, 1991, pp. 735-746.

[36]Hoekstra, A. J., Derksen, J. J., and Van den Akker, H. E. A., "An Experimental and Numerical Study of Turbulent Swirling Flow in Gas Cyclones," *Chemical Engineering Science,* Vol. 54, No. 13, 1999, pp. 2055-2065.

[37]Derksen, J. J., and Van den Akker, H. E. A., "Simulation of Vortex Core Precession in a Reverse-Flow Cyclone," *AIChE Journal,* Vol. 46, No. 7, 2000, pp. 1317-1331.

[38]Hu, L. Y., Zhou, L. X., Zhang, J., and Shi, M. X., "Studies of Strongly Swirling Flows in the Full Space of a Volute Cyclone Separator," *AIChE Journal,* Vol. 51, No. 3, 2005, pp. 740-749.

[39]Majdalani, J., and Saad, T., "The Taylor-Culick Profile with Arbitrary Headwall Injection," *Physics of Fluids,* Vol. 19, No. 9, 2007, pp. 093601-10.

[40]Majdalani, J., and Saad, T., "Energy Steepened States of the Taylor-Culick Profile," AIAA Paper 2007-5797, July 2007.

[41]Saad, T., and Majdalani, J., "The Taylor Profile in Porous Channels with Arbitrary Headwall Injection," AIAA Paper 2007-4120, June 2007.

[42]Saad, T., and Majdalani, J., "Energy Based Mean Flow Solutions for Slab Hybrid Rocket Chambers," AIAA Paper 2008-5021, July 2008.

[43]Majdalani, J., "On Steady Rotational High Speed Flows: The Compressible Taylor-Culick Profile," *Proceedings of the Royal Society, London, Series A,* Vol. 463, No. 2077, 2007, pp. 131-162.

[44]Vyas, A. B., Majdalani, J., and Chiaverini, M. J., "The Bidirectional Vortex. Part 1: An Exact Inviscid Solution," AIAA Paper 2003-5052, July 2003.